

Plasmon-phonon coupling in graphene

E. H. Hwang, Rajdeep Sensarma, and S. Das Sarma

Condensed Matter Theory Center, Department of Physics University of Maryland College Park, Maryland 20742-4111

(Dated: September 25, 2018)

Collective excitations of coupled electron-phonon systems are calculated for both monolayer and bilayer graphene, taking into account the non-perturbative Coulomb coupling between electronic excitations in graphene and the substrate longitudinal optical phonon modes. We find that the plasmon-phonon coupling in monolayer graphene is strong at all densities, but in bilayer graphene the coupling is significant only at high densities satisfying the resonant condition $\omega_{pl} \approx \omega_{ph}$. The difference arises from the peculiar screening properties associated with chirality of graphene. Plasmon-phonon coupling explains the measured quasi-linear plasmon dispersion in the long wavelength limit, thus resolving a puzzle in the experimental observations.

PACS numbers: 81.05.ue, 73.20.Mf, 71.38.-k, 63.22.Rc

A plasmon is a collective mode of charge-density oscillation in the free-carrier system, which is present both in classical and quantum plasmas. Studying the collective plasmon excitation in the electron gas has been among the very first theoretical quantum mechanical many-body problems studied in solid-state physics. The collective plasmon modes of monolayer graphene (MLG) have been extensively studied theoretically¹⁻⁶ and experimentally⁷⁻¹¹. Recent discovery of bilayer graphene (BLG) has also led to a number of theoretical descriptions of plasmon modes in BLG^{12,13}. Even though the long-wavelength plasmon frequency of MLG is explicitly nonclassical (i.e., the plasmon frequency is necessarily quantum with \hbar appearing manifestly in the long-wavelength plasma frequency³), its wave vector dispersion is given by classical electrodynamics, i.e., $\omega_p(q) \propto \sqrt{q}$. Note that the quadratic band-dispersion of BLG makes the leading order long-wavelength plasmon dispersion explicitly classical with the same $\sim \sqrt{q}$ dependence. However, at finite q , away from the long-wavelength limit, there are several corrections to the plasmon dispersion $\omega(q)$ arising from nonlocal finite wave vector response, finite-temperature thermal corrections, many-body effects, local-field corrections, and other mechanisms relevant to the specific electron system.

Since the plasmon dispersion relation is exactly known at long wavelengths ($q \rightarrow 0$) where the f-sum rule arising from particle conservation fixes the plasma frequency, it is surprising that the measured graphene plasmon dispersion in the long wavelength limit deviates from the classical dispersion ($\omega_q \sim \sqrt{q}$) and shows a rather linear dispersion^{8,10}. In a recent experiment⁹, the strongly coupled plasmon-phonon mode dispersion has been measured by the angle-resolved reflection electron-energy-loss spectroscopy and it is found that the discrepancy arises from electron-phonon coupling. In epitaxial graphene the substrate (i.e. SiC) is a highly polar material. In general, carriers in polar materials couple with the longitudinal optical (LO) phonons of the system via the long-range Fröhlich interaction. However, the surface optical (SO) phonon is a well-characterized surface property of polar semiconductors,

and it is possible that carriers in graphene layer couple to the SO-phonons of the underlying substrate lattice via the long-range polar Fröhlich coupling^{14,15}. For isotropic media the frequency of SO phonons ω_{SO} is related to the transverse optical (TO) bulk phonon ω_{TO} as $\omega_{SO}/\omega_{TO} = \sqrt{(\epsilon_0 + 1)/(\epsilon_\infty + 1)}$,¹⁴⁻¹⁶ where ϵ_0 (ϵ_∞) is the static (high frequency) dielectric constant. Note that the bulk longitudinal optical phonons ω_{LO} and ω_{TO} are connected with the dielectric constants by the Lyddane-Sachs-Teller relation $\omega_{LO}/\omega_{TO} = \sqrt{\epsilon_0/\epsilon_\infty}$.

The electron-phonon coupling is the macroscopic coupling of the electronic collective modes (plasmons) to the optical phonons. The mode coupling phenomenon, which hybridizes the collective plasmon modes of the electron gas with the optical-phonon modes of the lattice, gives rise to the coupled plasmon-phonon modes (the hybrid modes) which have been extensively studied¹⁷⁻²⁰ both experimentally and theoretically in bulk and 2D electron systems. The electron-phonon interaction leads to many-body renormalization of the single-particle free carrier properties^{21,22} and also affects the transport properties^{23,24}. A good understanding of electron-phonon coupling is thus important in developing quantitative theories for many different experimental studies in graphene.

In this paper we calculate the coupled plasmon-SO phonon modes of epitaxial graphene (or graphene on a polar substrate such as SiO₂, SiC, or HfO₂). Our most significant finding is that in MLG plasmon-phonon mode coupling effect is strong at all electronic densities due to the singular behavior in the screening function arising from chirality¹. By contrast, for BLG, the plasmon-phonon coupling is significant only at high carrier densities. We also find that at low densities, when the coupling is weak and the coupled phonon-like mode (gapped mode) lies in the interband electron-hole continuum, the energy of phonon-like mode decreases in the long wavelength limit due to the coupling of the phonon mode to the interband single particle excitation, which arises from the enhanced BLG backscattering²⁵. However, at high densities, when the plasmon-phonon mode coupling is strong, the phonon-like mode frequency increases linearly

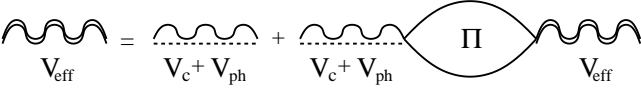


FIG. 1. Effective dynamical interaction V_{eff} calculated in RPA. Dashed (wiggly) lines represent the SO-phonon mediated (Coulomb) electron electron interaction V_{ph} (v_c), and the bubble the irreducible polarizability $\Pi(q, \omega)$.

with wavevector, as in MLG.

We first present our model for plasmon-phonon coupling, which consists of a two-dimensional electron gas coupled to dispersionless SO-phonons at zero temperature. For MLG, we have a system of Dirac fermions with linear dispersion, while BLG have a parabolic dispersion around the Dirac point. Due to the presence of the long range electron-phonon coupling, electrons interact among themselves through the Coulomb interaction and through virtual-SO-phonon exchange via the Fröhlich interaction. The electron-SO phonon interaction is given by

$$H_{e-ph} = \sum_{kq} \sum_{ss'} M_{kq}^{ss'} c_{k+qs}^\dagger c_{ks} (b_q + b_{-q}^\dagger), \quad (1)$$

where c_{ks}^\dagger is the electron ($s = +1$) or hole ($s = -1$) creation operator, b_q^\dagger and b_q are creation and destruction operators of surface phonon, and the interaction matrix element $M_{kq}^{ss'}$ is defined by

$$M_{kq}^{ss'} = M_0(q) F_{sk+q}^\dagger F_{s'k}, \quad (2)$$

where F_{sk} is the chiral spinor and given by $F_{sk}^\dagger = (s, e^{-i\theta_k})/\sqrt{2}$ with $s = \pm 1$, $\theta_k = \tan^{-1}(k_y/k_x)$ for MLG²⁶ and $\theta_k = 2 \tan^{-1}(k_y/k_x)$ for BLG^{27,28}. We also have

$$[M_0(q)]^2 = \frac{2\pi e^2}{q} e^{-2qd} \frac{\omega_{SO}}{2} \left[\frac{1}{\epsilon_\infty + 1} - \frac{1}{\epsilon_0 + 1} \right], \quad (3)$$

where d is the separation distance between graphene layer and substrate. Then the matrix element of SO-phonon mediated electron-electron interaction is dependent on both wave vector and frequency and give by,

$$v_{ph}(q, \omega) = [M_0(q)]^2 D_0(\omega), \quad (4)$$

where the unperturbed SO-phonon propagator is given by $D_0(\omega) = 2\omega_{SO}/(\omega^2 - \omega_{SO}^2)$.

The total effective electron-electron interaction is obtained in RPA¹⁹ by summing all the bare bubble diagrams (see Fig. 1),

$$v_{eff}(q, \omega) = \frac{v_c(q) + v_{ph}(q, \omega)}{1 - [v_c(q) + v_{ph}(q, \omega)] \Pi_0(q, \omega)} = \frac{v_c(q)}{\epsilon_t(q, \omega)} \quad (5)$$

where $v_c(q) = 2\pi e^2/\epsilon_\infty q$ is the electron-electron Coulomb interaction and $\Pi_0(q, \omega)$ is the complex irreducible polarizability of either the monolayer¹ or the bilayer system¹³ given by the bare bubble diagram. The

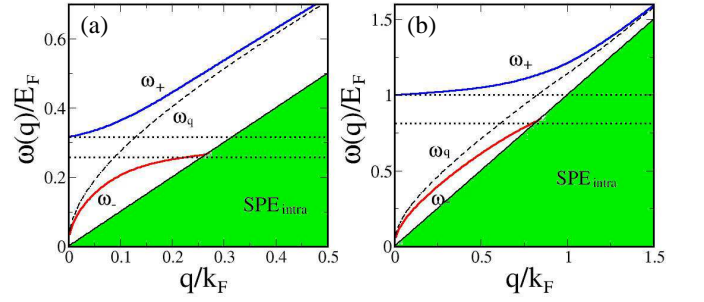


FIG. 2. Calculated plasmon-phonon coupled mode ω_{\pm} dispersions in MLG as a function of the wave vector q for two different densities (a) $n = 10^{13} \text{ cm}^{-2}$ and (b) $n = 10^{12} \text{ cm}^{-2}$. The plasmon dispersion (ω_q) without the electron-phonon coupling is shown by the dashed line. Two dotted horizontal lines represent the frequencies of the uncoupled SO (top) and TO (bottom) phonon modes, respectively.

total dielectric function within RPA contains contributions both from electrons and SO-phonons:

$$\epsilon_t(q, \omega) = 1 - \frac{2\pi e^2}{\epsilon_\infty q} \Pi_0(q, \omega) + \frac{\alpha e^{-2qd}}{1 - \alpha e^{-2qd} - \omega^2/\omega_{SO}^2}, \quad (6)$$

where

$$\alpha = \epsilon_\infty \left[\frac{1}{\epsilon_\infty + 1} - \frac{1}{\epsilon_0 + 1} \right]. \quad (7)$$

The collective mode dispersion is given by the zeros of the complex total dielectric function: $\epsilon_t(q, \omega) = 0$.

Let us first focus on the collective modes of MLG. In the long wavelength limit ($q \rightarrow 0$) we get the following coupled ω_{\pm} collective modes

$$\omega_+(q) = \omega_{SO} + \frac{\alpha e^{-2qd} \omega_q^2}{\omega_{SO}}, \quad (8a)$$

$$\omega_-(q) = (1 - \alpha e^{-2qd}) \omega_q, \quad (8b)$$

where $\omega_q^2 = 2e^2 E_F q / \epsilon_\infty$ ($E_F =$ Fermi energy) is the plasmon mode dispersion of an uncoupled system in the long wave length limit. As $q \rightarrow 0$ the phonon-like mode ω_+ is located above ω_{SO} and increases linearly, and the plasmon-like ω_- is slightly less than the corresponding uncoupled monolayer graphene plasmon mode, ω_q .

In Fig. 2 we show the calculated coupled plasmon-phonon collective modes in MLG for two different densities. The following parameters are used throughout this paper²⁹: $\omega_{TO} = 95.0 \text{ meV}$, $\omega_{SO} = 116.7 \text{ meV}$, $\epsilon_\infty = 6.4$, $\epsilon_0 = 10.0$, and $d = 5 \text{ \AA}$. As shown in Fig. 2 the mode coupling in MLG is strong for all electron densities. In ordinary 2D systems or 3D systems the plasmon-phonon mode coupling is only significant at densities satisfying the resonant condition $\omega_q \approx \omega_{SO}$. However, in MLG the plasmon mode exists for all wave vectors due to the singular behavior in the polarizability, which leads to strong plasmon-phonon coupling. Since the singular behavior of the polarizability arise from the suppression of the

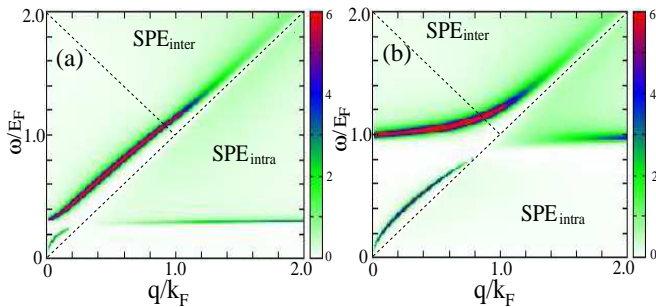


FIG. 3. The density plots of energy loss function ($-\text{Im}[1/\epsilon(q, \omega)]$) of MLG in (q, ω) space for two different densities (a) $n = 10^{13} \text{cm}^{-2}$ and (b) $n = 10^{12} \text{cm}^{-2}$. Note that the ω_+ mode of the high density result carries most spectral weight and its dispersion is almost linear, which is observed in the recent experiment⁸. We use a phenomenological damping of $0.1E_F$ in these results.

back scattering due to the chirality of MLG the strong plasmon-phonon coupling is a direct consequence of its unique chiral property of MLG. Note that the plasmon-like mode ω_- in Fig. 2 vanishes at a finite critical wave vector, $q_c \simeq \omega_{SO}(1 - \alpha)/v_F$, and for $q > q_c$ we find only the phonon-like mode (ω_+) which approaches ω_q for large q .

The dynamical structure factor, $S(q, \omega)$, which gives the spectral weight of the collective modes, is proportional to the imaginary part of the inverse dielectric function (loss function) and given by

$$S(q, \omega) = -\frac{1}{n_0 v_c(q)} \text{Im} \left[\frac{1}{\epsilon_t(q, \omega)} \right]. \quad (9)$$

For a true collective mode with zero Landau damping both $\text{Im}[\epsilon_t(q, \omega)]$ and $\text{Re}[\epsilon_t(q, \omega)]$ vanish, and the inverse dielectric function becomes a delta function with weight

$$W(q) = \frac{\pi}{\frac{\partial}{\partial \omega} \text{Re} \epsilon_t(q, \omega)|_{\omega=\omega_i(q)}} \quad (10)$$

where $\omega_i(q)$ is the collective mode frequency at wave vector q . In the long wavelength limit the weight of plasmon-like mode can be calculated as

$$W(q)|_{\omega_-} = \frac{\pi}{2} (1 - \alpha)^{3/2} \omega_q \quad (11)$$

and the weight of phonon-like mode as

$$W(q)|_{\omega_+} = \pi \alpha \omega_{SO} / 2. \quad (12)$$

The spectral weight of ω_- mode vanishes as \sqrt{q} in the long wavelength limit, but the weight of ω_+ mode is finite. Thus in the long wavelength limit all spectral weight is carried by the phonon-like mode. In Fig. 3 the calculated loss function $-\text{Im}[1/\epsilon(q, \omega)]$ is shown in (q, ω) space for two different densities (a) $n = 10^{13} \text{cm}^{-2}$ and (b) $n = 10^{12} \text{cm}^{-2}$. In the long wavelength limit the phonon-like mode has most of the weight. In the intermediate wave

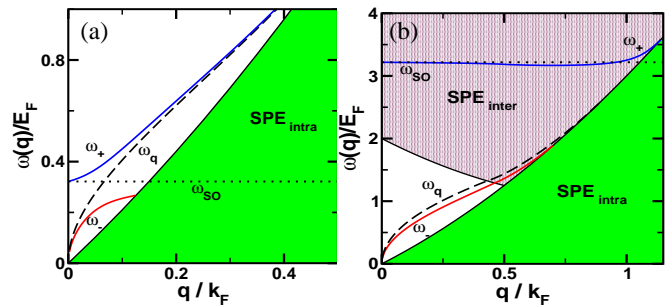


FIG. 4. Calculated plasmon-phonon coupled mode ω_{\pm} dispersions in bilayer graphene as a function of the wave vector q for two different densities (a) $n = 10^{13} \text{cm}^{-2}$ and (b) $n = 10^{12} \text{cm}^{-2}$. The plasmon dispersion (ω_q) without the electron-phonon coupling is shown by the dashed line. The dotted horizontal line represent the frequency of the uncoupled SO phonon mode.

vector range, however, the plasmon-like mode becomes stronger. The weight of the ω_- mode vanishes again when the plasmon-like mode merges with the electron-hole continuum at a critical wave vector and ω_- mode becomes overdamped by Landau damping.

Let us now turn our attention to BLG. Just like MLG, we again get two hybridized plasmon-phonon modes, one (ω_-) having a $\sim \sqrt{q}$ dispersion and the other (ω_+) exhibiting a gap equal to the SO phonon frequency (ω_{SO}) in the long wavelength limit. The ω_- mode has the same dispersion as in MLG, $\omega_-(q) = (1 - \alpha e^{-2qd})\omega_q$, which lies in the gap between the intraband and interband continua and has a spectral weight which goes as $\sim \sqrt{q}$. Thus, in the long wavelength limit, all the oscillator strength lies in the gapped mode ω_+ .

However, there are two main differences from MLG, i.e., the quadratic energy dispersion and the enhanced backscattering due to chirality in BLG²⁵, which lead to non-trivial differences in the collective mode spectrum. These two effects lead to very different behaviour in the low and high density limits. To illustrate these effects, we plot the collective mode spectrum of bilayer graphene at two different densities, (a) $n = 10^{13} \text{cm}^{-2}$ (high density, $E_F > \omega_{SO}$) and (b) $n = 10^{12} \text{cm}^{-2}$ (low density, $E_F < \omega_{SO}$) in Fig. 4. Here, ω_q is the uncoupled plasmon frequency and the shaded regions represent the intraband and interband particle-hole continuum. The corresponding loss functions are plotted in Fig. 5.

In the high density limit where $\omega_q \sim \omega_{SO}$, there is a strong plasmon-phonon coupling as evidenced by the deviations of ω_+ from ω_{SO} and of ω_- from ω_q , which gives rise to the gapped mode ω_+ having a linear dispersion with a positive slope in the low q limit. At larger q values, it approaches the uncoupled plasmon dispersion, as seen in Fig. 4(a). The ω_- mode merges into the continuum at a critical wavevector q_c , which is much smaller than that of the uncoupled mode indicating strong electron-phonon coupling. Furthermore, as seen from Fig. 5(a), the phonon-like mode ω_+ carries a much larger spectral

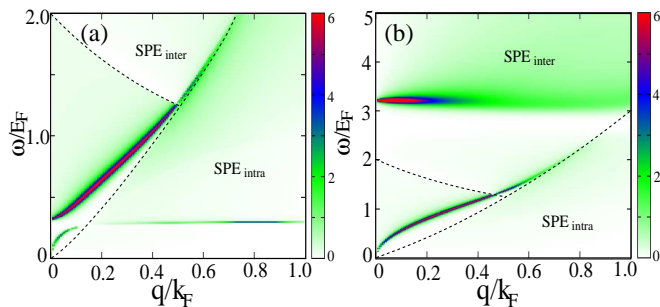


FIG. 5. The density plots of energy loss function ($-\text{Im}[1/\epsilon(q, \omega)]$) of bilayer graphene in (q, ω) space for two different densities (a) $n = 10^{13} \text{cm}^{-2}$ and (b) $n = 10^{12} \text{cm}^{-2}$.

weight than ω_- .

In the low density limit where $\omega_q < \omega_{SO}$, the plasmon-phonon coupling is weak and the gapped mode ω_+ is barely affected by the coupling. In addition, the mode energy decreases linearly in the long wave length limit, as seen in Fig. 4(b). The small negative slope is a consequence of the coupling of the phonon mode to the interband single particle excitation¹³ arising from the enhanced backscattering in the system and is a distinct difference between the MLG and BLG. Note that when the SO phonon mode is pushed into the interband electron-

hole continuum, the coupled ω_+ mode is always Landau-damped due to the presence of the interband continuum and carries little spectral weight beyond a very small range of low q values. The deviation of the plasmon-like mode ω_- from the uncoupled dispersion is much smaller than in the high density limit, further showing that the plasmon-phonon coupling is weak in this limit. From Fig. 5(b), we find that beyond a small range of low q values, the plasmon-like mode carries much more spectral weight than the phonon-like mode and hence, at low densities, the plasmon mode should be easier to detect in BLG.

In summary, we have calculated the dispersion and the spectral weight of the coupled plasmon-phonon mode of 2D graphene. We find that the mode-coupling effect is strong in monolayer graphene at all densities in contrast to the corresponding bilayer graphene, where the coupling is only significant at high densities. Since the carriers in graphene are strongly coupled to the surface optical phonon of a polar substrate it is important to understand the many-body renormalization of the single-particle properties and the transport properties in the presence of electron-SO phonon coupling.

This work is supported by ONR-MURI and SWANNRI.

-
- ¹ E. H. Hwang and S. Das Sarma, Phys. Rev. B **75**, 205418 (2007).
 - ² E. H. Hwang and S. Das Sarma, Phys. Rev. B **80**, 205405 (2009).
 - ³ S. Das Sarma and E. H. Hwang, Phys. Rev. Lett. **102**, 206412 (2009).
 - ⁴ B. Wunsch, T. Stauber, F. Sols, and F. Guinea, New J. Phys. **8**, 318 (2006).
 - ⁵ X.-F. Wang and T. Chakraborty, Phys. Rev. B **75**, 033408 (2007).
 - ⁶ O. Vafek, Phys. Rev. Lett. **97**, 266406 (2006).
 - ⁷ C. Kramberger, R. Hambach, C. Giorgetti, M. H. Rummeli, M. Knupfer, J. Fink, B. Büchner, L. Reining, E. Einarsson, S. Maruyama, F. Sottile, K. Hannewald, V. Olevano, A. G. Marinopoulos, and T. Pichler, Phys. Rev. Lett. **100**, 196803 (2008).
 - ⁸ Y. Liu, R. F. Willis, K. V. Emtsev, and T. Seyller, Phys. Rev. B **78**, 201403 (2008).
 - ⁹ Y. Liu and R. F. Willis, Phys. Rev. B **81**, 081406 (2010).
 - ¹⁰ T. Langer, J. Baringhaus, H. Pfnür, H. W. Schumacher, and C. Tegenkamp, New Journal of Physics **12**, 033017 (2010).
 - ¹¹ J. Lu, K. P. Loh, H. Huang, W. Chen, and A. T. S. Wee, Phys. Rev. B **80**, 113410 (2009).
 - ¹² G. Borghi, M. Polini, R. Asgari, and A. H. MacDonald, Phys. Rev. B **80**, 241402 (2009).
 - ¹³ R. Sensarma, E. H. Hwang, and S. Das Sarma, arXiv:1006.3078(2010).
 - ¹⁴ R. Fuchs and K. L. Kliewer, Phys. Rev. **140**, A2076 (1965).
 - ¹⁵ S. Q. Wang and G. D. Mahan, Phys. Rev. B **6**, 4517 (1972).
 - ¹⁶ L. H. Dubois and G. P. Schwartz, Phys. Rev. B **26**, 794 (1982).
 - ¹⁷ G. Abstreiter, M. Cardona, and A. Pinczuk, in *Light Scattering in Solids IV*, edited by M. Cardona and G. Gutherodt (Springer-Verlag, New York)(1984).
 - ¹⁸ R. Matz and H. Lüth, Phys. Rev. Lett. **46**, 500 (1981).
 - ¹⁹ R. Jalabert and S. Das Sarma, Phys. Rev. B **40**, 9723 (1989).
 - ²⁰ E. H. Hwang and S. Das Sarma, Phys. Rev. B **52**, R8668 (1995).
 - ²¹ W.-K. Tse, E. H. Hwang, and S. Das Sarma, Appl. Phys. Lett. **93**, 023128 (2008).
 - ²² C.-H. Park, F. Giustino, C. D. Spataru, M. L. Cohen, and S. G. Louie, Phys. Rev. Lett. **102**, 076803 (2009).
 - ²³ S. Fratini and F. Guinea, Phys. Rev. B **77**, 195415 (2008).
 - ²⁴ J. H. Chen, C. Jang, S. D. Xiao, M. Ishigami, and M. S. Fuhrer, Nature Nanotech. **3**, 206-209 (2008); K. Zou, X. Hong, D. Keefer, and Jun Zhu, arXiv:0912.1378.
 - ²⁵ E. H. Hwang and S. Das Sarma, Phys. Rev. Lett. **101**, 156802 (2008).
 - ²⁶ T. Ando, J. Phys. Soc. Jpn. **75**, 074716 (2006).
 - ²⁷ M. Koshino and T. Ando, Phys. Rev. B **73**, 245403 (2006).
 - ²⁸ E. McCann and V. I. Fal'ko, Phys. Rev. Lett. **96**, 086805 (2006).
 - ²⁹ H. Nienhaus, T. U. Kampen, and W. Mönch, Surf. Sci. **324**, L528 (1995).